Fusion of Evidences in Intensities Channels for Edge Detection in PolSAR Images

Anderson A. de Borba, Maurício Marengoni, and Alejandro C. Frery, *Senior Member, IEEE*

***Abstract*—Synthetic Polarimetric Aperture Radar (PolSAR) sensors have reached an essential position in remote sensing. The images they provide have speckle noise, making their processing and analysis challenging tasks. The present study discusses an edge detection method based on the fusion of evidence obtained in the intensity (hh), (hv), and (vv) channels of PolSAR multi-look images. The method consists of detecting transition points in the thinnest possible range of data that covers two regions using maximum likelihood under the Wishart distribution. The fusion methods used are simple average, multi-resolution discrete (MR-DWT) and stationary (MR-SWT) wavelet transforms, principal component analysis (PCA), ROC statistics, and a multi-resolution method based on singular value decomposition (MR-SVD). A quantitative analysis suggests that MR-SWT provides the best results.**

***Index Terms*—PolSAR, edge detection, maximum likelihood estimation, fusion methods.**

I. Introduction

POLARIMETRIC synthetic aperture radar (PolSAR) has achieved an essential position as a remote sensing technology. The data such sensors provide require specifically tailored signal processing techniques. Among such techniques, edge detection is one of the most important operations for extracting information. Edges are at a higher level of abstraction than mere data and, as such, provide relevant insights about the scene.

Among the available edge detection techniques for SAR and PolSAR images, it is worth mentioning:

- techniques based on denoising [1]–[5];
- Markov random fields [6];
- the deep learning approach [7], [8] applied to segmentation and classification; and,
- statistical techniques [9]–[11] applied in edge detection in PolSAR / SAR imagery.

This article follows the statistical modeling approach using the techniques described in [9]–[11] to find edge evidences, followed by fusion processes [12], [13]. Our approach does not attempt to reduce the speckle, but to extract information from its statistical properties.

Instead of handling fully polarimetric data, we treat each intensity channel separately, obtain evidence of edges, and then produce a single estimator of the edge position. With this, we quantify the contribution each channel provides to the solution of the problem.

We adopted the Gambini Algorithm [14], which consists in casting rays and then finding the evidence of an edge in the ray by maximizing a value function. The value function we use is the likelihood of two samples: one inside the edge, another outside the edge. Without loss of generality, we assume the complex scaled Wishart distribution for the fully polarimetric observations [15], from which Gamma laws stem for each intensity channel. The value function depends on the estimates that index such Gamma laws. We estimate them by maximum likelihood with the BFGS optimization method implemented in the `maxLik` package [16].

The value function is the total likelihood. It is non-differentiable at most points in the domain. It is known that classical methods have difficulties in finding the maximum of a non-differentiable functions. We used the Generalized Simulated Annealing (GenSA) [17] method to solve this problem.

We discuss six fusion methods:

- Simple average [12],
- Multi-Resolution Discrete Wavelet, MR-DWT [18],
- Principal Component Analysis, PCA [12], [18],
- ROC statistics [19], [20],
- Multi-Resolution Stationary Wavelet Transform, MR-SWT [18], [21], and
- Multi-Resolution Singular Value Decomposition, MR-SVD [22].

The article is structured as follows. Section II describes statistical modeling. Section II-A describes edge detection for PolSAR data. Section II-D describes the approach to edge evidence fusing. Section **??** presents numerical results. Finally, Section IV concludes the work with observations, future directions of research, and the feasibility of detecting edges in each channel of PolSAR images.

II. Methodology

Multi-looked fully polarimetric data follow the Wishart distribution with PDF defined by:

$$f_{\mathbf{Z}}(\mathbf{Z};\boldsymbol{\Sigma},L)=\frac{L^{mL}|\mathbf{Z}|^{L-m}}{|\boldsymbol{\Sigma}|^{L}\Gamma_m(L)}\exp(-L\,\mathrm{tr}(\boldsymbol{\Sigma}^{-1}\mathbf{Z})), \quad (1)$$

where, $\mathrm{tr}(\cdot)$ is the trace operator of a matrix, $\Gamma_m(L)$ is the multivariate Gamma function defined by $\Gamma_m(L) = \pi^{\frac{1}{2}m(m-1)}\prod_{i=0}^{m-1}\Gamma(L-i)$, and $\Gamma(\cdot)$ is the Gamma function. We used three $m=3$ channels in this study. This situation

A. A. de Borba is with the Dept. Engenharia Elétrica e Computação, Universidade Presbiteriana Mackenzie (UPM), and with IBMEC-SP, São Paulo, Brazil. anderson.borba@ibmec.edu.br

M. Marengoni is with the Dept. Engenharia Elétrica e Computação, UPM, São Paulo, Brazil. mauricio.marengoni@mackenzie.br

A. C. Frery is with the Laboratório de Computação Científica e Análise Numérica (LaCCAN), Universidade Federal de Alagoas (UFAL), Maceió, Brazil. acfrery@laccan.ufal.br

is denoted by $\mathbf{Z} \sim W(\mathbf{\Sigma}, L)$, which satisfies $E[\mathbf{Z}] = \mathbf{\Sigma}$. This assumption usually holds on targets where the speckle is fully developed but, since we will estimate L on each sample (instead of considering the same number of looks for the whole image), we will in part take into account departures from such hypothesis.

A. Sharp Edge Model

We approach edge detection with the Gambini Algorithm [9]–[11].

It consists of the following steps:

1) Identify the centroid of a region of interest (ROI) in an automatic, semi-automatic or manual manner.
2) Cast rays from the centroid to the outside of the area.
3) Collect data on a strip, ideally of the size of a pixel, around the rays using the Bresenham's midpoint line algorithm.
4) Compute the value function on every point of the ray.
5) Use the GenSA method [17], to find points of maxima in the functions of interest.
6) Fuse the evidence of detected edges in the (hh), (hv) and (vv) channels.

The value function is the reduced log-likelihood of the inner and external samples of the strip denoted, respectively, as $\boldsymbol{z}_{\mathrm{I}}$ and $\boldsymbol{z}_{\mathrm{E}}$. Each strip $\boldsymbol{z} = (z_1, z_2, \ldots, z_n)$ is, thus, partitioned in two disjoint samples at position j:

$$\boldsymbol{z} = (\underbrace{z_1, z_2, \ldots, z_j}_{\boldsymbol{z}_{\mathrm{I}}}, \underbrace{z_{j+1}, z_{j+2}, \ldots, z_n}_{\boldsymbol{z}_{\mathrm{E}}}).$$

We assume two (possibly) different models for each partition: $\boldsymbol{Z}_{\mathrm{I}} \sim \Gamma(\mu_{\mathrm{I}}, L_{\mathrm{I}})$, and $\boldsymbol{Z}_{\mathrm{E}} \sim \Gamma(\mu_e xtE, L_{\mathrm{E}})$. We then estimate $(\mu_{\mathrm{I}}, L_{\mathrm{I}})$ and $(\mu_{\mathrm{E}}, L_{\mathrm{E}})$ with $\boldsymbol{z}_{\mathrm{I}}$ and $\boldsymbol{z}_{\mathrm{E}}$, respectively, by maximizing (3), and obtain $(\widehat{\mu}_{\mathrm{I}}, \widehat{L}_{\mathrm{I}})$ and $(\widehat{\mu}_{\mathrm{E}}, \widehat{L}_{\mathrm{E}})$.

B. Marginal Models

Fully polarimetric data may be modeled by (1). Since we are interested in describing the information conveyed by parts of such matrix, we rely on the results presented in [23], [24].

1) Probability density Gamma function: We assume that the distribution of each intensity channel is a Gamma law with probability density function

$$f_Z(z; \mu, L) = \frac{L^L z^{L-1}}{\mu^L \Gamma(L)} \exp\big\{-Lz/\mu\big\}, \quad z > 0, \tag{2}$$

where $L > 0$ (rather than $L \geq 1$ to allow for flexibility), and $\mu > 0$ is the mean.

Given the sample $\boldsymbol{z} = (z_1, \ldots, z_n)$, the reduced log-likelihood of this model is

$$\ell(\boldsymbol{z}; L, \mu) = n\big[L\ln(L/\mu) - \ln\Gamma(L)\big] + L\sum_{k=1}^{n}\ln z_k - \frac{L}{\mu}\sum_{k=1}^{n} z_k. \tag{3}$$

We obtain $(\widehat{L}, \widehat{\mu})$, the maximum likelihood estimator (MLE) of (L, μ) based on $\boldsymbol{z}$, by maximizing (3) with the BFGS method implemented in the `maxLik` package [16]. We prefer optimization to solving $\nabla\ell = \mathbf{0}$ for improved numerical stability.

2) Probability density univariate magnitude of product: The magnitude of product σ_i e σ_j, where $i, j = \{\mathrm{HH}, \mathrm{HV}, \mathrm{VV}\}$, is an important measure of the polarimetric SAR image. Let normalized magnitude defined to,

$$z = \frac{\left|\frac{1}{L}\sum_{k=1}^{L}\sigma_i(k)\sigma_j^H(k)\right|}{\sqrt{E[|\sigma_i|^2]E[|\sigma_j|^2]}}. \tag{4}$$

The probability density univariate magnitude of product

$$f(z; \rho, L) = \frac{4L^{L+1}z^L}{\Gamma(L)(1-|\rho|^2)} I_0\left(\frac{2|\rho|Lz}{1-|\rho|^2}\right) K_{L-1}\left(\frac{2Lz}{1-|\rho|^2}\right), \tag{5}$$

where I_0 e K_{L-1} are modified Bessel functions, with $\rho > 0$, and $L > 0$.

Given the sample $z = (z_1, \ldots, z_n)$, the reduced log-likelihood of this model is

$$\begin{aligned}\ell(z; \rho, L) = {} & n\left[(L+1)\ln L - \ln\Gamma(L) - \ln(1-|\rho|^2)\right] \\ & + L\sum_{k=1}^{n}\ln z_k \\ & + \sum_{k=1}^{n}\ln I_0\left(\frac{2|\rho|Lz_k}{1-|\rho|^2}\right) \\ & + \sum_{k=1}^{n}\ln K_{L-1}\left(\frac{2Lz_k}{1-|\rho|^2}\right).\end{aligned} \tag{6}$$

3) Probability density univariate ratio intensity: The probability density ratio intensity among $\mathbf{S}_i$ e $\mathbf{S}_j$, where $i, j = \{\mathrm{HH}, \mathrm{HV}, \mathrm{VV}\}$, are important discriminators in the study of PolSar image. Let the normalized intensity ratio be

$$z = \frac{\sum_{k=1}^{n}\frac{|\sigma_i(k)|^2}{\Sigma_{11}}}{\sum_{k=1}^{n}\frac{|\sigma_j(k)|^2}{\Sigma_{22}}} = \frac{\sum_{k=1}^{n}|\sigma_i(k)|^2}{\tau\sum_{k=1}^{n}|\sigma_j(k)|^2}, \tag{7}$$

where $\tau = \frac{\Sigma_{11}}{\Sigma_{22}}$.

Considering the univariate probability density function ratio of multi-look intensities,

$$f(z; \rho, L) = \frac{\Gamma(2L)(1-|\rho|^2)^L(1+z)z^{L-1}}{\Gamma(L)\Gamma(L)\left[(1+z)^2 - 4|\rho|^2 z\right]^{\frac{2L+1}{2}}} \tag{8}$$

where, $\rho > 0$ and $L > 0$. Assuming

$$w = \frac{\sum_{k=1}^{n}\frac{|\sigma_i(k)|^2}{\Sigma_{11}}}{\sum_{k=1}^{n}\frac{|\sigma_j(k)|^2}{\Sigma_{22}}} = \tau z, \tag{9}$$

and performing the variable change in (8), we have

$$f(w; \rho, L, \tau) = \frac{\tau^L\Gamma(2L)(1-|\rho|^2)^L(\tau+w)w^{L-1}}{\Gamma(L)\Gamma(L)\left[(\tau+w)^2 - 4\tau|\rho|^2 w\right]^{\frac{2L+1}{2}}}. \tag{10}$$

The log-likelihood function is obtained by applying the natural logarithm in the equation (10)

$$\begin{aligned}\ell(\boldsymbol{w}; \rho, L, \tau) = {} & n\left(L\ln\tau + \ln\Gamma(2L) + L\ln(1-|\rho|^2)\right. \\ & \left. - 2\ln\Gamma(L)\right) + \sum_{k=1}^{n}\ln(\tau+w_k) + L\sum_{k=1}^{n}\ln w_k \\ & - \frac{2L+1}{2}\sum_{k=1}^{n}\ln\left[(\tau+w_k)^2 - 4\tau|\rho|^2 w_k\right]\end{aligned} \tag{11}$$

C. Edge Point Estimation

1) Probability density Gamma value function: The total log-likelihood at point j is, then,

$$\begin{aligned}\ell(j;\widehat{\mu}_I,\widehat{L}_I,\widehat{\mu}_E,\widehat{L}_E) &= j\big[\widehat{L}_{\mathrm{I}}\ln(\widehat{L}_{\mathrm{I}}/\widehat{\mu}_{\mathrm{I}})-\ln\Gamma(\widehat{L}_{\mathrm{I}})\big]\\ &+\widehat{L}_{\mathrm{I}}\sum_{k=1}^{j}\ln z_k-\frac{\widehat{L}_{\mathrm{I}}}{\widehat{\mu}_{\mathrm{I}}}\sum_{k=1}^{j}z_k\\ &+(n-j)\big[\widehat{L}_{\mathrm{E}}\ln(\widehat{L}_{\mathrm{E}}/\widehat{\mu}_{\mathrm{E}})-\ln\Gamma(\widehat{L}_{\mathrm{E}})\big]\\ &+\widehat{L}_{\mathrm{E}}\sum_{k=j+1}^{n}\ln z_k-\frac{\widehat{L}_{\mathrm{E}}}{\widehat{\mu}_{\mathrm{E}}}\sum_{k=j+1}^{n}z_k.\end{aligned} \tag{12}$$

We then apply GenSA to find

$$\widehat{\jmath}=\arg\max_{j\in[\min_s,N-\min_s]}\ell(j;\widehat{\mu}_I,\widehat{L}_I,\widehat{\mu}_E,\widehat{L}_E),$$

where $\min_s$ is a minimum sample size that we set to 14.

In this way, we obtain one estimates for the edge for each intensity channel. Notice that this approach can be extended and/or modified to cope with any kind of data.

2) Probability density magnitude of product value function: Using probability density magnitude of product value function (13) in the sample

$$\boldsymbol{z}=(\underbrace{z_1,z_2,\ldots,z_j}_{\boldsymbol{z}_{\mathrm{I}}},\underbrace{z_{j+1},z_{j+2},\ldots,z_n}_{\boldsymbol{z}_{\mathrm{E}}}).$$

We then estimate $(\rho_{\mathrm{I}},L_{\mathrm{I}})$ and $(\rho_{\mathrm{E}},L_{\mathrm{E}})$ with $\boldsymbol{z}_{\mathrm{I}}$ and $\boldsymbol{z}_{\mathrm{E}}$, respectively, by maximizing (13), and obtain $(\widehat{\rho}_{\mathrm{I}},\widehat{L}_{\mathrm{I}})$ and $(\widehat{\rho}_{\mathrm{E}},\widehat{L}_{\mathrm{E}})$.

The total log-likelihood at point j is, then

$$\begin{aligned}\ell(j;\widehat{\rho}_{\mathrm{I}},\widehat{L}_{\mathrm{I}},\widehat{\rho}_{\mathrm{E}},\widehat{L}_{\mathrm{E}}) = \\ &j\Big[(\widehat{L}_{\mathrm{I}}+1)\ln\widehat{L}_{\mathrm{I}}-\ln\Gamma(\widehat{L}_{\mathrm{I}})\\ &-\ln(1-|\widehat{\rho}_{\mathrm{I}}|^2)\Big]\\ &+\widehat{L}_{\mathrm{I}}\sum_{k=1}^{j}\ln z_k\\ &+\sum_{k=1}^{j}\ln I_0\left(\frac{2|\widehat{\rho}_{\mathrm{I}}|\widehat{L}_{\mathrm{I}}z_k}{1-|\widehat{\rho}_{\mathrm{I}}|^2}\right)\\ &+\sum_{k=1}^{j}\ln K_{\widehat{L}_{\mathrm{I}}-1}\left(\frac{2\widehat{L}_{\mathrm{I}}z_k}{1-|\widehat{\rho}_{\mathrm{I}}|^2}\right)\\ &+(n-j)\Big[(\widehat{L}_{\mathrm{E}}+1)\ln\widehat{L}_{\mathrm{E}}-\ln\Gamma(\widehat{L}_{\mathrm{E}})\\ &-\ln(1-|\widehat{\rho}_{\mathrm{E}}|^2)\Big]\\ &+\widehat{L}_{\mathrm{E}}\sum_{k=j+1}^{n}\ln z_k\\ &+\sum_{k=j+1}^{n}\ln I_0\left(\frac{2|\widehat{\rho}_{\mathrm{E}}|\widehat{L}_{\mathrm{E}}z_k}{1-|\widehat{\rho}_{\mathrm{E}}|^2}\right)\\ &+\sum_{k=j+1}^{n}\ln K_{\widehat{L}_{\mathrm{E}}-1}\left(\frac{2\widehat{L}_{\mathrm{E}}z_k}{1-|\widehat{\rho}_{\mathrm{E}}|^2}\right).\end{aligned} \tag{13}$$

We then apply GenSA to find

$$\widehat{\jmath}=\arg\max_{j\in[\min_s,N-\min_s]}\ell(j;\widehat{\rho}_I,\widehat{L}_I,\widehat{\rho}_E,\widehat{L}_E),$$

where $\min_s$ is a minimum sample size that we set to 14.

In this way, we obtain one estimates for the edge for each intensity channel. Notice that this approach can be extended and/or modified to cope with any kind of data.

We will see ways of fusing these evidences in the next section.

3) Probability density ratio intensity value function: Given the sample $\boldsymbol{w}=(w_1,\ldots,w_n)$, is to obtain $(\widehat{\rho},L,\widehat{\tau})$, the maximum likelihood estimator (MLE) of (ρ,L,τ) based on $\boldsymbol{w}$ maximizing (11) with the BFGS method implemented in the `maxLik` citeht package. We prefer optimization by solving $\nabla\ell=\mathbf{0}$ in order to improve numerical stability.

The function is the reduced log-likelihood for the internal and external samples of the data strip denoted respectively as $\boldsymbol{w}_{\mathrm{I}}$ and $\boldsymbol{w}_{\mathrm{E}}$. Each data strip $\boldsymbol{w}=(w_1,w_2,\ldots,w_n)$ is split into two disjointed samples at the j position:

$$\boldsymbol{w}=(\underbrace{w_1,w_2,\ldots,w_j}_{\boldsymbol{w}_{\mathrm{I}}},\underbrace{w_{j+1},w_{j+2},\ldots,w_n}_{\boldsymbol{w}_{\mathrm{E}}}).$$

The $(\rho_{\mathrm{I}},L_{\mathrm{I}},\tau_{\mathrm{I}})$ and $(\rho_{\mathrm{E}},L_{\mathrm{E}},\tau_{\mathrm{E}})$ with $\boldsymbol{w}_{\mathrm{I}}$ and $\boldsymbol{w}_{\mathrm{E}}$ are guested maximizing (6), to obtain $(\widehat{\rho}_{\mathrm{I}},\widehat{L}_{\mathrm{I}},\widehat{\tau}_{\mathrm{I}})$ and $(\widehat{\rho}_{\mathrm{E}},\widehat{L}_{\mathrm{E}},\widehat{\tau}_{\mathrm{E}})$.

The reduced log-likelihood in the point j is

$$\begin{aligned}\ell(j;\widehat{\rho}_{\mathrm{I}},\widehat{L}_{\mathrm{I}},\widehat{\tau}_{\mathrm{I}},\widehat{\rho}_{\mathrm{E}},\widehat{L}_{\mathrm{E}},\widehat{\tau}_{\mathrm{E}})&\\ =n\Big(\widehat{L}_{\mathrm{I}}\ln\widehat{\tau}_{\mathrm{I}}+\ln\Gamma(2\widehat{L}_{\mathrm{I}})&\\ +\widehat{L}_{\mathrm{I}}\ln(1-|\widehat{\rho}_{\mathrm{I}}|^2)-2\ln\Gamma(\widehat{L}_{\mathrm{I}})\Big)&\\ +\textstyle\sum_{k=1}^{n}\ln(\widehat{\tau}_{\mathrm{I}}+w_k)+\widehat{L}_{\mathrm{I}}\sum_{k=1}^{n}\ln w_k&\\ -\frac{2\widehat{L}_{\mathrm{I}}+1}{2}\textstyle\sum_{k=1}^{n}\ln\left[(\widehat{\tau}_{\mathrm{I}}+w_k)^2-4\widehat{\tau}_{\mathrm{I}}|\widehat{\rho}_I|^2w_k\right]&\\ +n\Big(\widehat{L}_{\mathrm{E}}\ln\widehat{\tau}_{\mathrm{E}}+\ln\Gamma(2\widehat{L}_{\mathrm{E}})&\\ +\widehat{L}_{\mathrm{E}}\ln(1-|\widehat{\rho}_{\mathrm{E}}|^2)-2\ln\Gamma(\widehat{L}_{\mathrm{E}})\Big)&\\ +\textstyle\sum_{k=1}^{n}\ln(\widehat{\tau}_{\mathrm{E}}+w_k)+\widehat{L}_{\mathrm{E}}\sum_{k=1}^{n}\ln w_k&\\ -\frac{2\widehat{L}_{\mathrm{E}}+1}{2}\textstyle\sum_{k=1}^{n}\ln\left[(\widehat{\tau}_{\mathrm{E}}+w_k)^2-4\widehat{\tau}_{\mathrm{E}}|\widehat{\rho}_{\mathrm{E}}|^2w_k\right]&\end{aligned} \tag{14}$$

Vamos aplicar o método GenSA para encontrar

$$\widehat{\jmath}=\arg\max_{j\in[\min_s,N-\min_s]}\ell(j;\widehat{\rho}_I,\widehat{L}_I,\widehat{\tau}_I,\widehat{\rho}_E,\widehat{L}_E,\widehat{\tau}_E),$$

onde $\min_s$ é o tamanho mínimo da amostra definido por 14.

Desta maneira, vamos obter uma estimativa para a borda em cada canal de intensidade. Note que esse método pode ser estendido e/ou modificado para lidar com qualquer tipo de dados.

D. Fusion of Evidences

Denote in the following $\widehat{\boldsymbol{\jmath}}_c$ the binary image with same support as the input data c (m lines and n columns; denote $\ell=mn$), where 1 denotes an estimate of edge and 0 otherwise. We have n_c of these image to fuse, and the result of the fusion will be denoted $\boldsymbol{I}_F$.

We compare the results of six fusion techniques, namely: simple average, multi-resolution discrete wavelet transform (MR-DWT), principal components analysis (PCA), ROC statistics, multi-resolution stationary wavelet transform (MR-SWT), and multi-resolution singular value decomposition (MR-SVD).

1) Simple Average: The simple average fusion method proposes the arithmetic mean of the edge evidence in each of the n_c channels: $\boldsymbol{I}_F(x,y) = (n_c)^{-1}\sum_{c=1}^{n_c}\widehat{\boldsymbol{\jmath}}_c(x,y)$.

2) Multi-Resolution Discrete Wavelet – MR-DWT: This section is based on [18]. We apply DWT filters on each binary image $\widehat{\boldsymbol{\jmath}}_c$: a low-pass filter $\boldsymbol{L}$ in the vertical direction, and a high-pass filter $\boldsymbol{H}$ in the horizontal direction, then both are down-sampled to create the coefficient matrices $\widehat{\boldsymbol{\jmath}}_{c\mathrm{L}}$ and $\widehat{\boldsymbol{\jmath}}_{c\mathrm{H}}$. These operations are repeated on the coefficient matrices, leading to $\widehat{\boldsymbol{\jmath}}_{c\mathrm{LL}}$, $\widehat{\boldsymbol{\jmath}}_{c\mathrm{LH}}$, $\widehat{\boldsymbol{\jmath}}_{c\mathrm{HL}}$, and $\widehat{\boldsymbol{\jmath}}_{c\mathrm{HH}}$.

The DWT fusion method has the following steps:

1) Calculate the DWT decomposition $\widehat{\boldsymbol{\jmath}}_{c\mathrm{LL}}$, $\widehat{\boldsymbol{\jmath}}_{c\mathrm{LH}}$, $\widehat{\boldsymbol{\jmath}}_{c\mathrm{HL}}$, and $\widehat{\boldsymbol{\jmath}}_{c\mathrm{HH}}$, for each channel.
2) Compute $\bar{\boldsymbol{\jmath}}_{c\mathrm{HH}}$, the pixel-wise mean of all $\widehat{\boldsymbol{\jmath}}_{c\mathrm{HH}}$ decompositions.
3) Find the pixel-wise maximum of $\widehat{\boldsymbol{\jmath}}_{c\mathrm{LL}}$, $\widehat{\boldsymbol{\jmath}}_{c\mathrm{LH}}$, $\widehat{\boldsymbol{\jmath}}_{c\mathrm{HL}}$: $\bar{\boldsymbol{\jmath}}_{c\mathrm{LL}}$, $\bar{\boldsymbol{\jmath}}_{c\mathrm{LH}}$, and $\bar{\boldsymbol{\jmath}}_{c\mathrm{HL}}$.
4) The result of the fusion I_F is the inverse DWT transformation of the coefficient matrices $\bar{\boldsymbol{\jmath}}_{c\mathrm{HH}}$, $\bar{\boldsymbol{\jmath}}_{c\mathrm{LL}}$, $\bar{\boldsymbol{\jmath}}_{c\mathrm{LH}}$, and $\bar{\boldsymbol{\jmath}}_{c\mathrm{HL}}$.

3) Principal Component Analysis – PCA: This section is based on [12], [18]. The method is comprised of the following steps:

1) Stack the binary images $\widehat{\boldsymbol{\jmath}}_c$ in column vectors to obtain the matrix $\boldsymbol{X}_{\ell\times n_c}$.
2) Calculate the covariance matrix $\boldsymbol{C}_{n_c\times n_c}$ of $\boldsymbol{X}_{\ell\times n_c}$.
3) Compute the matrices of eigenvalues ($\boldsymbol{\Lambda}$) and eigenvectors ($\boldsymbol{V}$) of the covariance matrix, sorted in decreasing order by the eigenvalues.
4) Compute the components $\boldsymbol{P}_c = (\sum_{m=1}^{n_c}\boldsymbol{V}_c(m))^{-1}\boldsymbol{V}_c$, where $\boldsymbol{V}_c$ is eigenvector associated with the highest eigenvalue of $\boldsymbol{X}$; notice that $\sum_{c=1}^{n_c}\boldsymbol{P}_c = 1$.
5) Fuse $\boldsymbol{I}_F(x,y) = \sum_{c=1}^{n_c}\boldsymbol{P}_c\widehat{\boldsymbol{\jmath}}_c(x,y)$.

4) ROC Statistics: The ROC method was proposed and described on [19], [20]:

1) Add the binary images $\widehat{\boldsymbol{\jmath}}_c$ to produce the frequency matrix ($\boldsymbol{V}$).
2) Use thresholds ranging from $t = 1,\ldots,n_c$ on $\boldsymbol{V}$ to generate matrices $\boldsymbol{M}_t$.
3) Compare each $\boldsymbol{M}_t$ with all $\widehat{\boldsymbol{\jmath}}_c$, find the confusion matrix to generate the ROC curve. The optimal threshold corresponds to the point of the ROC curve closest (in the sense of the Euclidean distance) to the diagnostic line.
4) The fusion $\boldsymbol{I}_F$ is the matrix $\boldsymbol{M}_t$ which corresponds to the optimal threshold.

5) Multi-Resolution Stationary Wavelet Transform – MR-SWT: This section is based on [18], [21]. The difference between MR-DWT and MR-SWT method is the replacement of the method discrete wavelet transform (DWT) by the method stationary wavelet transform SWT.

6) Multi-Resolution Singular Value Decomposition – MR-SVD: MR-SVD Fusion [22] works similarly to MR-DWT. The difference consists in changing the DWT filters by the SVD filters. The MR-SVD fusion method can be summarized as follows:

1) Organize the binary image $\widehat{\boldsymbol{\jmath}}_c$ as non-overlapping 2×2 blocks, and arrange each block as a 4×1 vector by stacking columns to form the data matrix $\boldsymbol{X}_1$ with dimension $4\times\ell/4$.
2) Find the SVD decomposition of $\boldsymbol{X}_1 = \boldsymbol{U}_1\boldsymbol{S}_1\boldsymbol{V}_1^T$, where $\boldsymbol{U}_1$ and $\boldsymbol{V}_1$ are unitary and they have dimensions 4×4 e $\ell/4\times\ell/4$ respectively. The diagonal entries S_{ii} of $\boldsymbol{S}_1$ are known as the singular values of $\boldsymbol{X}_1$ and it have dimension $4\times\ell/4$. The singular values are sorted in descending, and they are putting in the diagonal principal of the matrix, other entries must be zeros.
3) Transform the lines of $\widehat{\boldsymbol{X}_1} = \boldsymbol{U}_1^T\boldsymbol{X}_1 = \boldsymbol{S}_1\boldsymbol{V}_1^T$ into new matrices with dimensions $m/2\times n/2$: $\{\boldsymbol{\Phi}_1,\boldsymbol{\Psi}_{1\mathrm{V}},\boldsymbol{\Psi}_{1\mathrm{H}},\boldsymbol{\Psi}_{1\mathrm{D}}\}$.
4) Repeat the procedure (1) on $\boldsymbol{\Phi}_r$ by $r = 2$ up to the lowest resolution level R.
5) The MR-SVD decomposition in each channel is

$$\widehat{\boldsymbol{X}_c} \rightarrow \left\{\boldsymbol{\Phi}_{\mathrm{R}}^c, \{\boldsymbol{\Psi}_{r\mathrm{V}}^c, \boldsymbol{\Psi}_{r\mathrm{H}}^c, \boldsymbol{\Psi}_{r\mathrm{D}}^c\}_{r=1}^{\mathrm{R}}, \{\boldsymbol{U}_r^c\}_{r=1}^{\mathrm{R}}\right\}.$$

6) Once the decomposition is applied to all channels, compute the average of $\boldsymbol{\Phi}_R^c$ ($\boldsymbol{\Phi}_{\mathrm{R}}^f$) in the lowest resolution level, and the average of $\boldsymbol{U}_r^c$ ($\boldsymbol{U}_{\mathrm{r}}^f$), for each r, where f denotes the fusion among channels.
7) Find the pixel-wise maxima of $\boldsymbol{\Psi}_{r\mathrm{V}}^c$, $\boldsymbol{\Psi}_{r\mathrm{H}}^c$ and $\boldsymbol{\Psi}_{r\mathrm{D}}^c$: $\boldsymbol{\Psi}_{rV}^f$ $\boldsymbol{\Psi}_{r\mathrm{V}}^f$, $\boldsymbol{\Psi}_{r\mathrm{H}}^f$ and $\boldsymbol{\Psi}_{r\mathrm{D}}^f$.
8) The fusion $\boldsymbol{I}_F$ is the SVD transformation for each level $r = \mathrm{R},\ldots,1$,

$$\boldsymbol{I}_F \leftarrow \left\{\boldsymbol{\Phi}_{\mathrm{R}}^f, \{\boldsymbol{\Psi}_{r\mathrm{V}}^f, \boldsymbol{\Psi}_{r\mathrm{H}}^f, \boldsymbol{\Psi}_{r\mathrm{D}}^f\}_{r=\mathrm{R}}^{1}, \{\boldsymbol{U}_r^f\}_{r=\mathrm{R}}^{1}\right\}.$$

III. Results

A. Simulated Image

Figure (3)(a) shows the log-likelihood function to simulated image with radial equal to 50 and the fixed point in sample k from 1 to 100, and Figure (3)(b) is similar with the fixed point in sample k from 100 to 400.

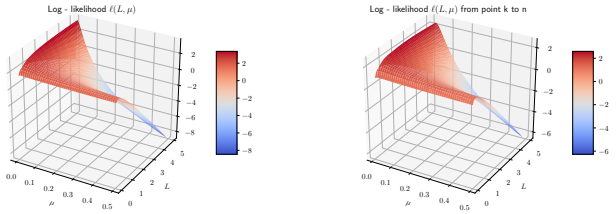

(a) Pixel from 1 to k. (b) Pixel from k+1 to n .

Fig. 1. Log-likelihood gamma function to simulated image.

Figures (2)(a)(b)(c) shows evidence edges to simulated image in each channel.

B. PolSAR Image

We used a 750×1024 pixels AIRSAR PolSAR image of Flevoland, L-band, for the tests. Fig. shows the ROI, with the radial lines where edges are detected. Fig. 4b shows the ground reference in red.

Figs. 5(a), 5(b), and 5(c) show, respectively, the edge evidences in the hh, hv and vv channels as obtained by MLE.

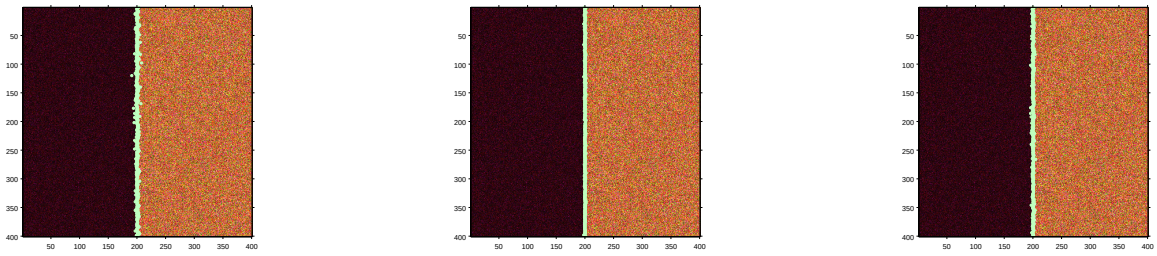

(a) Evidences in channel hh (b) Evidences in channel hv (c) Evidences in channel vv

Fig. 2. Edges evidences from the three intensity channels

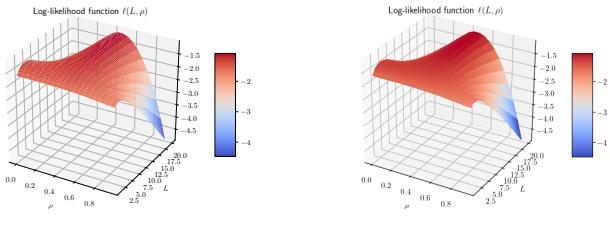

(a) Pixel from 1 to k. (b) Pixel from k+1 to n .

Fig. 3. Log-likelihood gamma function to simulated image.

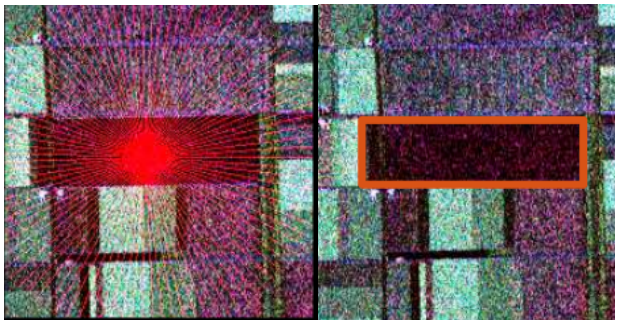

(a) Image, Region of Interest (ROI), and rays. (b) Ground reference

Fig. 4. Flevoland image in Pauli decomposition, region of interest, and ground reference

It is worth noting that GenSA has accurately identified the maximum value of ℓ (14), even in the presence of multiple local maxima. A visual assessment leads to conclude that the best results are provided by hv, although with a few points far from the actual edge.

Figs. 6(a), (b), (c), (d), (e), and (f) show the results of fusing these evidences.

The simple average and PCA produce similar results. MR-SVD produces considerably less outliers than the other methods, at the cost of longer processing time. ROC produces accurate edges, with few outliers, but sparsely. Both wavelet-based methods (DWT and SWT) produce too dense edges and many outliers.

Figure 7 shows the error of $\widehat{j}$ in finding the true edge, as measured on 100 radial lines: the minimum Euclidean distance among the ground truth pixel and the several pixels detected in the fusion methods. We use relative frequencies to estimate the probability of having an error smaller than a number of pixels. Denoting $H(k)$ the number of replications for which the error is less than k pixels, an estimate of this probability is $f(k) = H(k)/n_r$, where n_r is the radial number. In our analysis, k varies between 1 and 10. The algorithm is described in Ref. [10].

C. Implementation Details

The system presented here was executed on a Intel© Core i7-9750HQ CPU 2.6 GHz 16 GB RAM computer. The method for detecting edge evidence MLE was implemented in the R language. The fusion methods were implemented in Matlab.

Table I shows the running times (absolute and relative to the fastest method).

TABLE I
PROCESSING TIMES (FUSION METHOD).

Method	Aver	PCA	MR-DWT	MR-SWT	ROC	MR-SVD
Time (s)	0.01	0.02	0.08	0.18	0.40	1.11
Rel. time	1.00	2.19	9.25	21.05	46.59	129.57

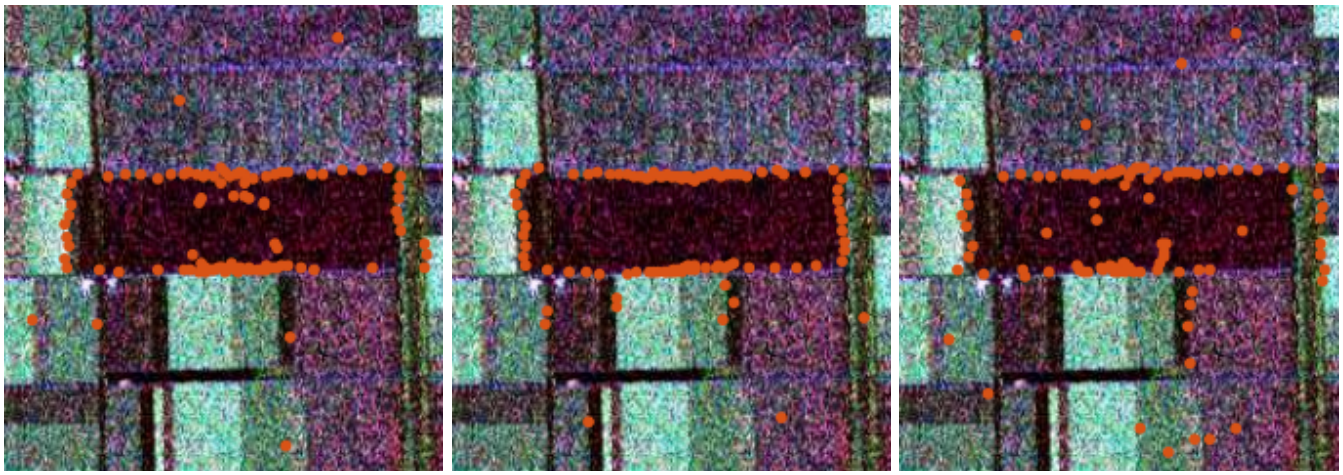

(a) Evidences in channel hh (b) Evidences in channel hv (c) Evidences in channel vv

Fig. 5. Edges evidences from the three intensity channels

IV. Discussion

We found evidence of edges using the maximum likelihood method under the Wishart model for PolSAR data. The evidence was found in each of the three intensity channels of an AIRSAR L-band image over Flevoland.

The best edge evidence was observed on the hv channel. We assessed the result by checking the closeness of the fused points to the actual edge, by the presence of outliers, and by the blurring effect.

We applied simple average, MR-DWT, PCA, ROC, MR-SWT, and MR-SVD fusion methods to aggregate the evidence obtained in the three channels. The best result was produced by the Multi-Resolution Stationary Wavelet Transform (MR-SWT) with a moderate cost of the processing time.

We highlight two avenues for future improvement of the fusion:

1) increasing the number of evidences. This is possible, since fully polarimetric data is richer than mere intensity channels; and
2) post-processing of both partial evidences and fusion.

References

[1] J. Shi, H. Jin, and Z. Xiao, "A novel hybrid edge detection method for polarimetric SAR images," *IEEE Access*, vol. 8, pp. 8974–8991, 2020.

[2] B. Liu, Z. Zhang, X. Liu, and W. Yu, "Edge extraction for polarimetric SAR images using degenerate filter with weighted maximum likelihood estimation," *IEEE Geoscience and Remote Sensing Letters*, vol. 11, no. 12, pp. 2140–2144, Dec 2014.

[3] W. Wang, D. Xiang, Y. Ban, J. Zhang, and J. Wan, "Enhanced edge detection for polarimetric SAR images using a directional span-driven adaptive window," *International Journal of Remote Sensing*, vol. 39, no. 19, pp. 6340–6357, 2018.

[4] J. Lee, T. L. Ainsworth, and Y. Wang, "A review of polarimetric SAR speckle filtering," in *2017 IEEE International Geoscience and Remote Sensing Symposium (IGARSS)*, July 2017, pp. 5303–5306.

[5] D. Santana-Cedrés, L. Gomez, L. Alvarez, and A. C. Frery, "Despeckling PolSAR images with a structure tensor filter," *IEEE Geoscience and Remote Sensing Letters*, vol. 17, no. 2, pp. 357–361, Feb 2020.

[6] F. Baselice and G. Ferraioli, "Statistical edge detection in urban areas exploiting SAR complex data," *IEEE Geoscience and Remote Sensing Letters*, vol. 9, no. 2, pp. 185–189, March 2012.

[7] J. E. Ball, D. T. Anderson, and C. S. Chan, "Comprehensive survey of deep learning in remote sensing: theories, tools, and challenges for the community," *Journal of Applied Remote Sensing*, vol. 11, no. 04, p. 1, sep 2017.

[8] X. X. Zhu, D. Tuia, L. Mou, G. Xia, L. Zhang, F. Xu, and F. Fraundorfer, "Deep learning in remote sensing: A comprehensive review and list of resources," *IEEE Geoscience and Remote Sensing Magazine*, vol. 5, no. 4, pp. 8–36, Dec 2017.

[9] J. Gambini, M. Mejail, J. Jacobo-Berlles, and A. C. Frery, "Feature extraction in speckled imagery using dynamic B-spline deformable contours under the G0 model," *International Journal of Remote Sensing*, vol. 27, no. 22, pp. 5037–5059, 2006.

[10] A. C. Frery, J. Jacobo-Berlles, J. Gambini, and M. Mejail, "Polarimetric SAR image segmentation with B-Splines and a new statistical model," *Multidimensional Systems and Signal Processing*, vol. 21, pp. 319–342, 2010.

[11] A. Nascimento, M. Horta, A. Frery, and R. Cintra, "Comparing edge detection methods based on stochastic entropies and distances for PolSAR imagery," *Journal of Selected Topics in Applied Earth Observations and Remote Sensing*, vol. 7, no. 2, pp. 648–663, 2014.

[12] H. Mitchell, *Image Fusion: Theories, Techniques and Applications*. Springer Berlin Heidelberg, 2010.

[13] A. A. de Borba, M. Marengoni, and A. C. Frery, "Fusion of evidences for edge detection in PolSAR images," in *2019 IEEE Recent Advances in Geoscience and Remote Sensing: Technologies, Standards and Applications (TENGARSS)*, Oct 2019, pp. 80–85.

[14] J. Gambini, M. Mejail, J. Jacobo-Berlles, and A. C. Frery, "Accuracy of edge detection methods with local information in speckled imagery," *Statistics and Computing*, vol. 18, no. 1, pp. 15–26, 2008.

[15] S. N. Anfinsen, A. P. Doulgeris, and T. Eltoft, "Estimation of the equivalent number of looks in polarimetric synthetic aperture radar imagery," *IEEE Transactions on Geoscience and Remote Sensing*, vol. 47, no. 11, pp. 3795–3809, 2009.

[16] A. Henningsen and O. Toomet, "maxlik: A package for maximum likelihood estimation in R," *Computational Statistics*, vol. 26, no. 3, pp. 443–458, 2011.

[17] Y. Xiang, S. Gubian, B. Suomela, and J. Hoeng, "Generalized Simulated Annealing for Global Optimization: The GenSA Package," *The R Journal*, vol. 5, no. 1, pp. 13–28, 2013.

[18] V. Naidu and J. Raol, "Pixel-level image fusion using wavelets and principal component analysis," *Defence Science Journal*, vol. 58, pp. 338–352, Mar. 2008.

[19] S. Giannarou and T. Stathaki, "Optimal edge detection using multiple operators for image understanding," *EURASIP Journal on Advances in Signal Processing*, vol. 2011, no. 1, p. 28, Jul 2011.

[20] T. Fawcett, "An introduction to ROC analysis," *Pattern Recogn. Lett.*, vol. 27, no. 8, pp. 861–874, Jun. 2006.

[21] Q. Jiang, X. Jin, S. Lee, and S. Yao, "A novel multi-focus image fusion method based on stationary wavelet transform and local features of fuzzy sets," *IEEE Access*, vol. 5, pp. 20 286–20 302, 2017.

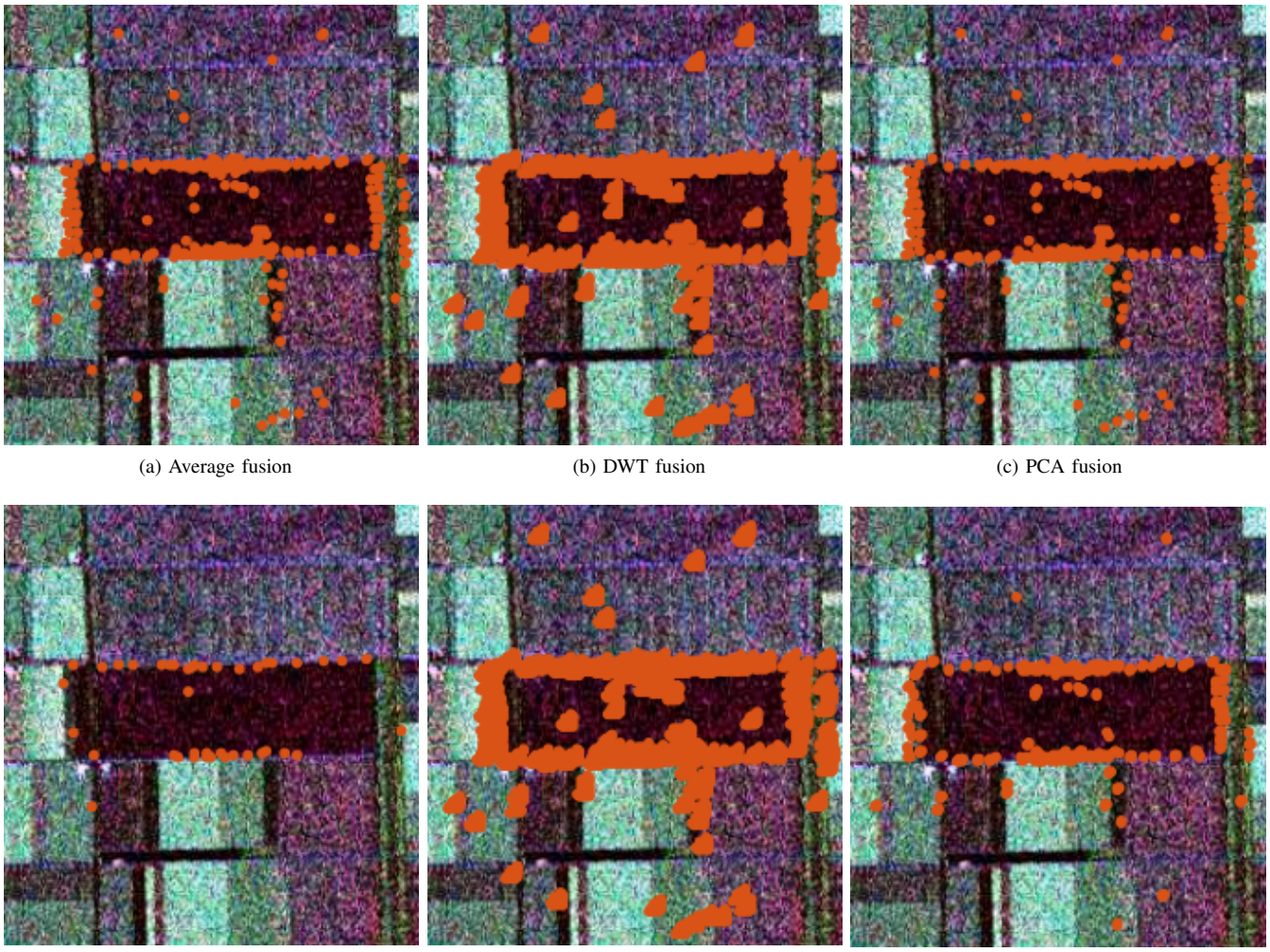

(a) Average fusion (b) DWT fusion (c) PCA fusion

(d) ROC fusion (e) MR-SWT fusion (f) MR-SVD fusion

Fig. 6. Results of applying the six fusion methods

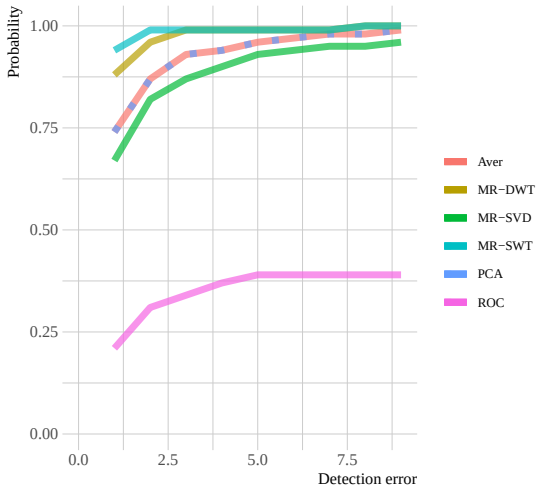

Fig. 7. Probability of detecting in fusion methods.

[22] V. Naidu, "Image fusion technique using multi-resolution singular value decomposition," *Defence Science Journal*, vol. 61, no. 5, pp. 479–484, Sep. 2011.

[23] J. S. Lee, K. W. Hoppel, S. A. Mango, and A. R. Miller, "Intensity and phase statistics of multilook polarimetric and interferometric SAR imagery," *IEEE Transactions on Geoscience and Remote Sensing*, vol. 32, no. 5, pp. 1017–1028, Sep. 1994.

[24] M. Hagedorn, P. Smith, P. Bones, R. Millane, and D. Pairman, "A trivariate chi-squared distribution derived from the complex Wishart distribution," *Journal of Multivariate Analysis*, vol. 97, no. 3, pp. 655–674, 2006.